

Nonlinear electrophoretic velocity of DNA in slitlike confinementMichael Lamontagne¹ and Stephen Levy*Department of Physics, Applied Physics and Astronomy, Binghamton University, 4400 Vestal Parkway East, P.O. Box 6000, Binghamton, New York 13902-6000, USA*

(Received 22 December 2021; accepted 20 April 2022; published 11 May 2022)

We have applied zero-time-averaged alternating electric fields to DNA molecules in a cross-shaped nanofluidic slit. We observed a net drift of DNA molecules, the magnitude of which depends on the square of the electric field amplitude. From the rate of accumulation of DNA at the center of the device, we derive an estimate for the second-order electrophoretic mobility, μ_2 . We observe that focusing is absent at a dipole rotation frequency >20 Hz, which suggests that μ_2 depends on the frequency of the alternating fields. The observation of a nonzero μ_2 raises the possibility of frequency-dependent electrophoretic DNA separation by length achievable in the absence of a sieving matrix.

DOI: [10.1103/PhysRevE.105.054503](https://doi.org/10.1103/PhysRevE.105.054503)**I. INTRODUCTION**

The theory of polyelectrolyte electrophoresis has a long and complicated history [1–3]. Particularly for highly charged semiflexible biopolymers, like double-stranded DNA, there is still considerable uncertainty about which approximations are appropriate in finding an analytical expression for the electrophoretic mobility [4]. The complications arise from several interrelated factors, discussed in some detail by Hoagland *et al.* [5].

To briefly summarize, the origin of one of the complications is the so-called diffuse counterion cloud that surrounds the polyelectrolyte out to the Debye length, which depends inversely on the square root of the ion concentration [6]. In this discussion, we consider a solution with added salt as in our experiment. In a salty solution, the Coulomb interaction between point charges is exponentially screened by the Debye length in the limit of the linearized Poisson-Boltzmann equation for small surface potentials [7]. Under the application of an external electric field, the counterions are driven with a force equal in magnitude to the electric force on the polyelectrolyte and opposite in direction. The force transmitted to the polyelectrolyte through the viscous medium is less, however, since the hydrodynamic interactions are screened over a similar scale [1]. Another more important complication, in the context of our experiment, results when the symmetry of the diffuse counterion cloud is deformed due to the motion of the polyelectrolyte with respect to the solvent. This effect has traditionally been termed “relaxation,” or “asymmetry field,” and it results in a slowing of the polyelectrolyte due effectively to the dipole distribution of the ion cloud that opposes the applied field [8]. The force transmitted to the polyelectrolyte through the solvent by the motion of the ion cloud previously discussed must be corrected due to the distortions in the cloud. Consequently, there is a complicated dependence on the polyelectrolyte mobility with the ionic concentration.

For long DNA molecules in a monovalent salt solution, it has been observed experimentally that the mobility decreases monotonically with the ionic strength [5].

The importance of several of these complications is lessened when one is able to linearize the Poisson-Boltzmann equation for small surface potentials. This approximation does not appear valid on its face for double-stranded DNA with two negative charges every base pair (0.34 nm) when in an aqueous solution with neutral pH. Manning’s theory of counterion condensation [9], however, posits that the charge on a polyelectrolyte in a salt solution is renormalized by the counterions when the spacing between charges is less than the Bjerrum length. The Bjerrum length equates the Coulomb energy of two unit charges in solution to the thermal energy. For DNA, this indicates that its bare charge should be reduced by about 75% from its nominal value [10] making the Debye-Hückel approximation more reasonable. However, while helpful in explaining some observed aspects of polyelectrolyte dynamics [11], the counterion condensation theory has been criticized for containing unphysical assumptions [4].

Electrophoresis of DNA within a confining fluidic structure, such as a nanoslit, adds more complications to the story. The confining structure modulates the conformation and dynamics of the DNA in ways that have been extensively studied in experiment, theory, and simulation [12–15]. The most relevant aspects for our experiment result from the extension of the DNA molecule’s equilibrium size and the increase in its longest relaxation time with the confining slit height (h). According to the de Gennes blob model in moderate slit confinement, the equilibrium size and the longest relaxation time scale as $h^{-1/4}$ and $h^{-7/6}$, respectively [16]. Additionally, since the confining slit walls are negatively charged in aqueous solution in our experiment, the ionic double layer that extends approximately a Debye length from the walls can be important. This double layer can overlap at low salt concentration or small slit heights, though we are far from that realm in our experiment. More importantly, the applied external electric field can drive bulk fluid flow through electroosmosis due to the convection of the positive salt ions in the double layer near the

*mlamont1@binghamton.edu

walls (in the direction opposite to that of the electrophoretic force on the DNA) [6].

To summarize, the most relevant issues of polyelectrolyte electrophoresis for our experiment result from the relaxation of the diffuse ions surrounding a DNA molecule as well as the DNA relaxation time being a function of the confining slit height. It should further be noted that theories of electrophoresis do not consider changes to the equilibrium conformation of the polyelectrolyte at moderate electric field strengths. However, Tang *et al.* [17] showed that coupling of electrohydrodynamic flows can cause compression of individual DNA molecules in bulk under constant applied electric fields.

II. THEORY

We investigate the possibility that the DNA electrophoretic velocity (v) depends nonlinearly on the electric field (\vec{E}). Experiments such as those done by Campbell [18] indicate that, though the electrophoretic velocity is commonly assumed to be proportional to the electric field in free solution, statistically significant deviations from linearity are observed for λ DNA confined in nanocapillaries with dimensions in the 100–500 nm range. We therefore make the assumption that

$$\vec{v} = (\mu_1 + \mu_2 E) \vec{E}, \quad (1)$$

where E is the magnitude of \vec{E} , and μ_1 is the commonly referred to electrophoretic mobility. The concentration of DNA exploiting this nonlinear dependence of electrophoretic velocity on electric field has previously been demonstrated in an agarose gel [19,20]. Following a similar method, we apply an electric field that consists of the superposition of a dipole field (\vec{E}_d) rotating at angular frequency ω and a quadrupole field (\vec{E}_q) rotating at 2ω . The dipole field is given by

$$\vec{E}_D = E_{0D} [\cos(\omega t) \hat{x} + \sin(\omega t) \hat{y}]. \quad (2)$$

The coordinate system is shown overlaid on a schematic of the central region of the cross-shaped slit in Fig. 1. The magnitude E_{0D} is $E_{0D} = \Delta V/L$, where L is the distance separating two electrodes. The quadrupole field is given by

$$\vec{E}_Q = -E_{0Q} \cos(2\omega t) [x\hat{x} - y\hat{y}], \quad (3)$$

where x and y are the horizontal and vertical distance from the origin, respectively. The magnitude E_{0Q} is complicated by the geometry of the device used in the experiment. In our device, E_{0Q} is approximately equal to $(E_{0D}/80 \mu\text{m})$ within the central region (Fig. 1), as further detailed in the Discussion section. Substituting $\vec{E} = \vec{E}_D + \vec{E}_Q$ into Eq. (1) and taking the time average, we see that the term proportional to μ_1 will not contribute. The term proportional to μ_2 , however, is significantly more complicated. It can be shown [21] that the time-averaged velocity in the limit that $E_{0D} \gg E_{0Q}$ is given by

$$\langle \vec{v} \rangle = -\frac{1}{4} \mu_2 E_{0D} E_{0Q} \vec{r}, \quad (4)$$

where \vec{r} is the radial vector in two dimensions. We refer to this configuration of fields as *focusing* because DNA molecules at nonzero \vec{r} will on average drift radially toward the center.

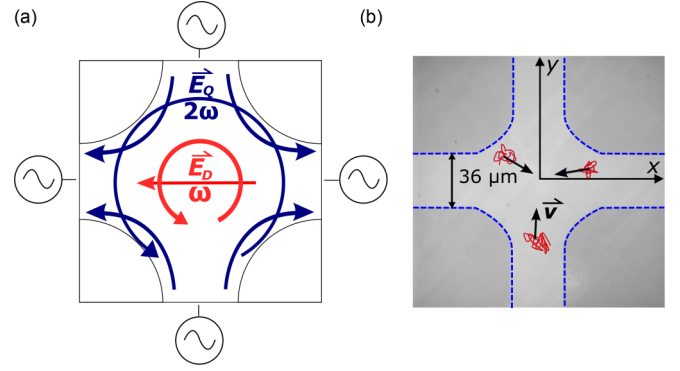


FIG. 1. (a) Schematic of the rotating quadrupole (blue) and the rotating dipole (red) electric fields that are summed to create the *focusing* field orientation within the central region of the cross-nanoslit device. The four legs extend 0.75 cm and terminate in fluid reservoirs where electrodes are inserted in order to apply the fields (not shown). (b) An optical micrograph of the central region at 40 \times magnification taken in brightfield with the walls of the device traced (blue-dashed line). A cartoon of DNA molecules is overlaid (red), showing the direction of the drift velocity of each molecule (radially inward) during the application of the focusing field.

If we change the initial phase of the quadrupole field such that

$$\vec{E}_Q = E_{0Q} \cos(2\omega t) [x\hat{x} - y\hat{y}], \quad (5)$$

then the time-averaged velocity in the limit that $E_{0D} \gg E_{0Q}$ is given by

$$\langle \vec{v} \rangle = \frac{1}{4} \mu_2 E_{0D} E_{0Q} \vec{r}. \quad (6)$$

We refer to this mode as *defocusing* because molecules not at the center should drift radially outward from the center on average. The results for the time-averaged drift velocity in Eqs. (4) and (6) were confirmed by numerical integration of Eq. (1) in the described limit.

The focusing and defocusing behavior were qualitatively confirmed in a simple computer simulation written in PYTHON. The simulation employed a Runge-Kutta method to update the trajectory of a point particle subject to electrophoretic drift from the combined dipole and quadrupole field, and thermal diffusion for a lambda DNA molecule in an approximately 250-nm-deep slit based on experimental results [16].

We note that if we assume the velocity has a nonlinear dependence on the electric field as shown in Eq. (1), the time-averaged velocity for either the dipole field alone ($\vec{E} = \vec{E}_D$) or the quadrupole field alone ($\vec{E} = \vec{E}_Q$) is zero. This result is straightforward for $\vec{E} = \vec{E}_D$. When $\vec{E} = \vec{E}_Q$, the result depends on the time average of $|\cos(2\omega t)| \cos(2\omega t)$ being zero.

III. EXPERIMENTAL SECTION

Devices were fabricated on 500- μm -thick double-sided polished fused silica wafers (Mark Optics) using standard contact photolithographic techniques. The nanoslits were reactive ion etched using a CHF₃-O₂ plasma (Oxford Instruments), then measured using a Dektak-150 profilometer. A nanofluidic device consisted of four perpendicular legs that

were each 0.75 cm long, 36 μm wide, and approximately 253 nm deep. The legs were oriented perpendicular to each other such that they formed a cross. The interior corners of their intersection, which we refer to as the central region, were rounded hyperbolically to avoid edge effect artifacts in the applied electric fields, the equation of the hyperbola being $y = 1000 \mu\text{m}^2/x$. The hyperbolic curve of the walls extended in the domain $20 < |x| < 50 \mu\text{m}$. At distances greater than 50 μm from the center, y was constant and the legs had a constant width. Each leg terminated in an access hole, made via sandblasting. Here a reservoir for fluid and a gold electrode could be inserted. We refer to the four reservoirs for a given device as left, right, top, and bottom. The etched wafer was cleaned and touch bonded to a fused silica cover wafer (160 μm thick, Mark Optics), then slowly heated to 1050 $^\circ\text{C}$ in a Thermo Scientific Lindberg/Blue M box furnace to make the bond permanent.

Fluid reservoirs were formed by gluing pipette tips, with the ends removed, using 732 silicone rubber sealant (Dow Corning) over the access holes. The buffer consisted of 445 mM Tris-borate and 10 mM EDTA (5 \times TBE), with 3% by volume β -mercaptoethanol added to reduce photobleaching. The ionic strength of this buffer is estimated to be about 160 mM.

λ DNA (48.5 kbp, New England Biolabs) was prepared at a concentration of 1.6×10^{-10} M and stained with YOYO-1 dye (Thermo Fisher Scientific) at a ratio of 5:1 bp:dye molecules. In a typical focusing experiment, 3 μL of stained λ DNA was added to 57 μL of 5X-TBE in the left reservoir. In a typical defocusing experiment, 10 μL of stained λ DNA solution was added to 50 μL of buffer in the left reservoir in order to increase the ambient concentration of DNA in the central region. DNA was loaded into the channel overnight with a 45 V/cm electric field applied between the left and right reservoirs.

The electrode potentials were applied using a National Instruments PCI-6229 DAQ card controlled by LabView, and amplified by four LTC2057HV op amps (Linear Technology), chosen for their small input offset voltage and low thermal offset output drift. Electrical contact was made with the buffer in the reservoirs using gold electrodes.

A dipole field is created by applying a potential difference between opposite legs (left-right or top-bottom). A quadrupole field is created by applying a symmetric potential difference (e.g., +30 and -30 V) between perpendicular legs (left-top, right-top, left-bottom, and right-bottom), and zero potential difference between opposite legs (left-right or top-bottom). The dipole and quadrupole fields are shown schematically in Fig. 1(a). In both focusing ($\vec{E} = \vec{E}_D + \vec{E}_Q$) and defocusing ($\vec{E} = \vec{E}_D - \vec{E}_Q$) configurations, we used a value of 3π rad/s for ω (the dipole was rotated at a frequency of 1.5 Hz, and the quadrupole at 3 Hz). The instantaneous sum of the quadrupole and dipole potentials was rounded to one of four discretization values for convenience. Each discrete potential was held for a length of time equal to 1/12th of a dipole period (T), as shown in Fig. 2. $T/12$ was chosen as the time interval for discretization arbitrarily. The discrete voltage values for the focusing orientation were +15, 0, -15 , and -30 V. For the defocusing orientation, the values were +28,

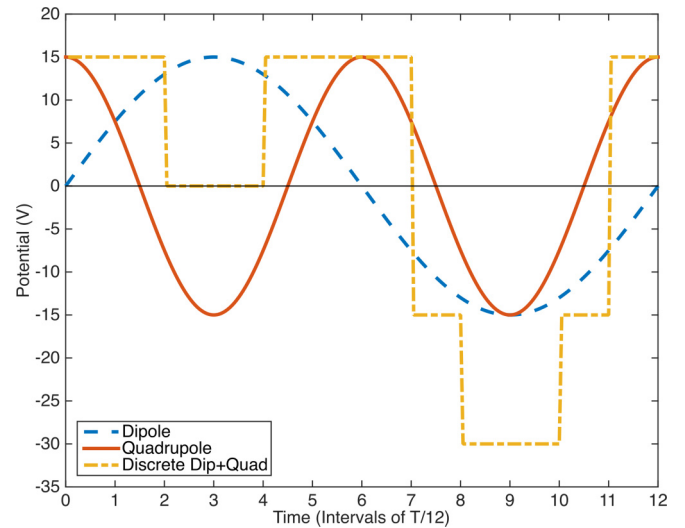


FIG. 2. The potential pattern applied to one electrode in the focusing configuration. The mathematical quadrupole (red, solid) and dipole (blue, dashed) potentials are summed and discretized to four possible outputs (+15, 0, -15 , or -30 V) as represented by the square wave (yellow, dot-dashed). Despite being asymmetric in time, the discretized dipole plus quadrupole potential integrates to zero over one dipole period.

+14, 0, and -14 V. The values are not symmetric because the superposed field is also asymmetric in time, as shown in Fig. 2.

To eliminate capacitive coupling leading to small biases in the drift of the DNA, 24 American Wire Gauge shielded tray cable (Automation Direct) was used to connect the DAQ to the printed circuit board (PCB) where the amplifiers were mounted. Additionally, a ground plane was added between traces on the front and back of the PCB, and signal traces were kept a minimum of 1 cm apart. The circuit board was designed in Autodesk Eagle and fabricated by OSH PARK.

The fluorescent DNA was observed using an Evolve EM-CCD camera (Photometrics) connected to an Olympus IX71 inverting microscope using a 40 \times , 0.75 numerical aperture objective (Olympus). An X-Cite Series 120PC mercury lamp was used to excite the YOYO dye. Images were taken with an exposure time of 140 ms using a custom LabView program approximately every 15 min and processed using custom software written in MATLAB.

Between experiments, the buffer was removed from the reservoirs, replaced with DI water, and the reservoirs were covered with parafilm to prevent evaporation. Intermittent blockages of the entrance to the nanoslit in the reservoir region were cleared with dilute sulfuric acid (1.8 M) if we were unsuccessful in loading DNA after several trials. Afterwards, the devices were rinsed repeatedly with 5X-TBE and allowed to equilibrate for at least 24 h before the next experiment.

IV. RESULTS

We experimentally observed DNA entering the central region during the application of the focusing field configuration with $\omega = 3\pi$ rad/s (1.5 Hz dipole frequency) over the course of 22 h. The amount of DNA in the central region increased

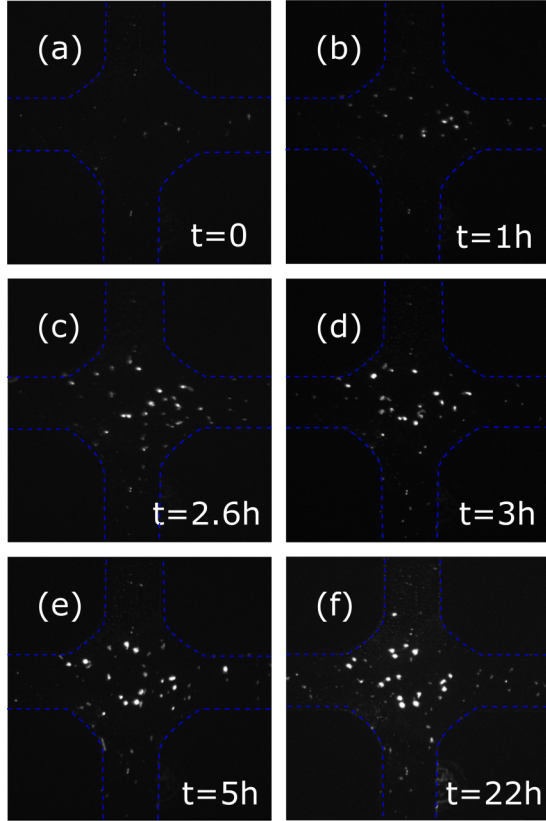


FIG. 3. (a) Fluorescent image of the central region of the cross-slit showing λ DNA at the start of the application of the focusing field orientation rotating at a dipole frequency of 1.5 Hz. Walls are traced (blue-dashed line). Magnification is $40\times$. Fluorescent image of the central region after applying the focusing field for 1 h (b), 2.6 h (c), 3 h (d), 5 h (e), and 22 h (f). Although fragments of λ DNA are evident, a clear increase in the fluorescent intensity, or DNA concentration, is observed over time.

linearly over time after approximately 1 h, as shown in Fig. 3. Images were taken roughly every 15 min for 5 h. The fields were applied for an additional 17 h without the 15 min interval images being taken, after which the final images were taken, as shown in Fig. 3(f).

To establish that the focusing effect was caused by the superposition of the dipole and quadrupole fields rather than either in isolation, experiments were conducted with $\vec{E} = \vec{E}_Q$ and separately with $\vec{E} = \vec{E}_D$, with $\omega = 3\pi$ rad/s in each case. A negligible amount of DNA was seen to enter the central region during the application of each, as seen in Fig. 4. Occasionally, a DNA molecule was observed to stick to the surface of the glass. These were removed by applying a 45 V/cm field from left to right for about 15 s. Images containing stuck DNA were not used in the analysis.

The rate of accumulation of DNA in the focusing configuration was determined using a custom MATLAB algorithm. To select for regions containing fluorescently labeled λ DNA, each frame was binarized so that pixels below an intensity threshold were revalued at 0, while those above the threshold were revalued at 1. The threshold intensity was determined by averaging Otsu's method [22] over several images from

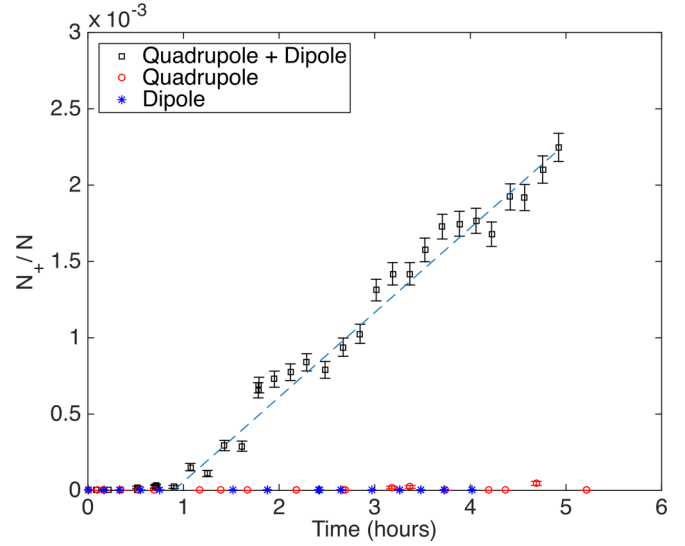


FIG. 4. Plot of the fraction of connected pixels passing a brightness threshold in images of the central region over time for the focusing (quadrupole and dipole) field (black squares), quadrupole-only (red circle), and dipole-only (blue star) fields. The data are fit to a linear function by a least-squares estimate (blue-dashed line).

near the middle of the focusing experiment. In addition, bright objects below an area of five connected pixels were removed to eliminate camera noise. We refer to the number of pixels that pass these criteria as N_+ . We refer to the total number of pixels in an image as N . We then plotted the ratio N_+/N versus the time from the start of the experiment, as shown in Fig. 4. The data used to calculate the best-fit line were from images taken after the first DNA molecule, passing the previously discussed criteria, was seen to enter the central region (~ 1 h). The uncertainty was determined from a binomial distribution algorithm for the observed probability of N_+ bright pixels appearing in a sequence of N binary pixels. The slope of the best-fit line in the focusing experiment was $(5.39 \pm 0.17) \times 10^{-4}$ / h, where the uncertainty represents the standard error. The slope of the best-fit line in the defocusing experiment was $(-1.92 \pm 0.20) \times 10^{-3}$ / h.

V. DISCUSSION

DNA was seen to accumulate in the central region during the application of the focusing orientation of fields as seen in Fig. 4. The rate (R) at which DNA molecules were entering the central region during the application of the focusing fields was determined from the slope of the best linear fit ($\Delta N_+ / \Delta t$) as follows:

$$R = \frac{1}{A} \frac{\Delta N_+}{\Delta t}, \quad (7)$$

where A is the average area of a DNA molecule in the central region. From the rate, we extracted an estimate for μ_2 using the following expression derived from Eq. (4):

$$\mu_2 \approx \frac{2 R L}{E_{0D} E_{0Q} r}, \quad (8)$$

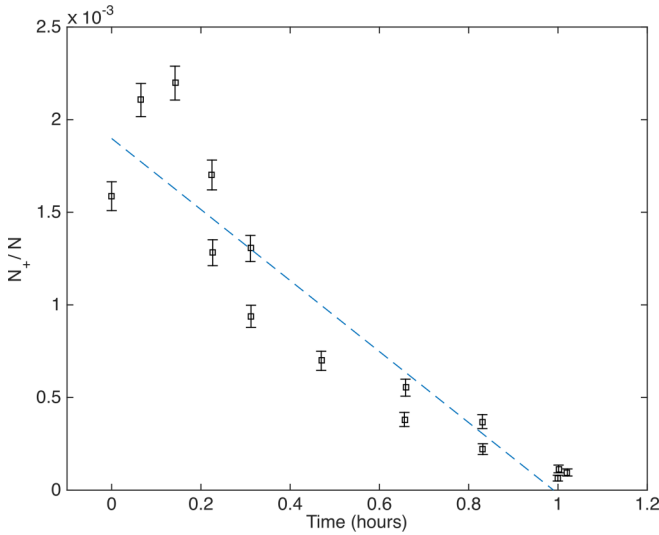


FIG. 5. Plot of the fraction of connected pixels passing a brightness threshold in images of the central region over time for the defocusing (dipole and inverted quadrupole) field. The data are fit to a linear function by a least-squares estimate (blue-dashed line).

where L is the average distance between DNA molecules projected onto the x - y plane (parallel to the confining slit walls), representing the average interparticle distance before the application of the focusing fields, and r is the radial distance from the origin to the border of the central region. The factor of 2 in the numerator results from DNA being able to enter the central region from either the left or right.

The average area of a molecule of λ DNA in the central region was found to be 42 ± 19 pixels, corresponding to approximately $6 \mu\text{m}^2$. No attempt was made to correct for the point spread function of the optical system, as we are only seeking an order-of-magnitude estimate. Using L inferred from the loading concentration of the DNA and the cross-sectional area of the channel, we estimate $\mu_2 = 1.5 \times 10^{-6} \text{ cm}^3/(\text{V}^2 \text{ s})$. The separation of molecules along the loading axis was observed to be about 7% larger than the calculated value. We note that this value of μ_2 implies that the speed of DNA would be about double its known value in a dc field [23] at $\sim 270 \text{ V/cm}$. The somewhat higher estimate for μ_2 than we expected adds further credence to our conclusion that the emergence of a nonlinearity in v may be frequency-dependent, since it has not previously been observed in similar experiments in bulk solution or in a confined geometry with dc fields.

Additionally, the DNA concentration in the central region was observed to decrease with time during the application of the defocusing field as seen in Fig. 5. Accordingly, we determined an estimate for μ_2 based on the best fit ($\Delta N_+/\Delta t$) for the rate of DNA exit from the images taken during the application of the defocusing field using the following expression:

$$\mu_2 \approx \frac{-RL}{E_{0D} E_{0Q} r}. \quad (9)$$

The factor of 2, relative to Eq. (8), results from the DNA being able to exit the central region through all four legs. This expression gives an estimate of $\mu_2 = 1.7 \times 10^{-6} \text{ cm}^3/(\text{V}^2 \text{ s})$. We believe that the larger spread in the data at the start of the application of the defocusing fields is an artifact of the loading concentration of the DNA being larger than in the focusing experiment. The higher loading concentration was chosen to ensure that a significant amount of DNA would be present within the central region before the application of the fields.

The first-order mobility (μ_1) of λ DNA was also measured within our cross nanoslit device. Videos were taken of several molecules moving electrophoretically under a constant electric field with magnitude ranging between 10 and 30 V/cm. The velocities were determined via custom particle tracking software in MATLAB. The first-order mobility was found to be $(2.41 \pm 0.15) \times 10^{-5} \text{ cm}^2/\text{V s}$. This value differs significantly from the mobility value for long DNA in bulk [23]. The first-order mobility at approximately this degree of confinement has previously [18,24] been measured to be about $9 \times 10^{-5} \text{ cm}^2/\text{V s}$. The difference is likely due to an increase in electroosmotic flow in our experiment. We conducted an additional experiment at lower salt concentration using 1 \times -TBE as the buffer. The DNA molecules were then observed to move toward the lower potential electrode in the loading field, leading us to conclude that the electro-osmotic flow was larger than the electrophoretic force at this salt concentration. Other researchers have added polyvinylpyrrolidone (PVP) to the buffer in nanochannel devices to suppress the electroosmotic flow [24,25]. However, it was demonstrated that the PVP can act like a sieving matrix [26], introducing an additional source of nonlinearity in the electrophoretic velocity of DNA molecules. Previous experiments also indicate that the observed mobility can vary significantly from day-to-day [27,28].

There are several approximations in our analysis. We used a finite-difference method numerical solution to the Poisson equation in two dimensions to evaluate the dipole and quadrupole fields separately. The dipole field is not uniform in the entire central region. The necessity of having a limited width-to-height ratio in a nanofluidic slit to prevent collapse when bonding introduces a limitation that would not be present were the dipole field to fill a full two-dimensional square region. The numerical model indicates that the magnitude of the dipole field in the legs perpendicular to the dipole direction decays exponentially with a decay length of approximately $80 \mu\text{m}$. This decay in the off-axis dipole magnitude puts a limit on the distance from which DNA can be effectively focused in the cross nanoslit.

The numerical model of the quadrupole field indicates that it is zero at the origin and linearly rises to approximately the same magnitude as the on-axis dipole field within about two channel widths ($80 \mu\text{m}$) of the origin, where it remains constant. It is known that the quadrupole field is extensional in the central region [29] (i.e., the field strength along a given axis is proportional to the distance along that axis). The electric field lines in the central region were qualitatively verified to approximate a quadrupole by following tracer DNA moving under a constant applied quadrupole field. As discussed in the supplemental material [21], Eq. (4) for the drift velocity is only exact when the magnitude of the quadrupole (E_{0Q}) is

much smaller than the magnitude of the dipole (E_{0D}), which is approximately true within the central region.

It is possible that the physical properties of the buffer could change as it is heated by the electrical current passing through it in such a way as to make v appear nonlinear with E , as is the case in high field experiments in agarose [30]. We calculate a projected rise in temperature (T) per time (t) due to Joule heating in our experiment of

$$\frac{\Delta T}{t} = \frac{F V_{\text{rms}}^2}{R C m} \approx 3 \times 10^{-3} \text{ }^\circ\text{C/h}, \quad (10)$$

where V_{rms} is the root-mean-square voltage, C is the specific heat of water (4184 J/kg K), R is the resistance of the nanoslit (measured to be $\approx 4000 \text{ M}\Omega$), m is the mass of buffer in the nanoslits and reservoirs, and F is a unit conversion factor. It then seems quite unlikely that Joule heating plays a role in the inception of μ_2 over the 5 h interval in our experiment. We also ignore the possible complicated effect of intermolecular DNA interactions within the central region, which may need to be included in future measurements of higher precision. We note that the maximum concentration of DNA achieved in the central region still appears to be lower than the crossover into the semidilute regime where inter polymer entangling has traditionally been considered to start [31], and therefore we consider it unlikely to play a role.

We also investigated the frequency dependence of μ_2 in a limited range due to experimental constraints. Though Eq. (4) did not predict a dependence of μ_2 on the dipole frequency, the 1.5 Hz dipole frequency at which the experiments were performed was chosen as it is slightly higher than the frequency at which focusing was observed in more viscous agarose by Marziali *et al.* [20]. As shown in Fig. 1 in the supplemental material [21], the focusing effect in our device was not observed at a dipole frequency $>20 \text{ Hz}$ over a 6 h period. We surmise that the relaxation time of the DNA, approximately 0.5 s for lambda DNA in a 250-nm-deep slit [16], may play a role in the frequency dependence of μ_2 . Additionally, the extended conformation of the DNA in the confining slit may affect the relaxation time of the surrounding diffuse ion cloud, as discussed previously. We therefore consider it likely that there is a resonant frequency, affected by the depth of the confining slit and DNA contour length, at which DNA focusing is most effective. The lower limit of the explorable frequency range is set by the width of the central region. At too low a frequency, the molecule is carried a significant distance outside the central region, where the approximation of $E_{0D} \gg E_{0Q}$ no longer holds, and the focusing drift speed is not well characterized. The width of the central region could likely be slightly increased in the future without causing the collapse of the channels.

The drift velocity within the central region was found to be too small to be well characterized when tracking a single molecule due to the time limit set by eventual photobleaching of the molecule. Single molecule observations should be possible in the future in a device with a wider central region, or increased electric field strength across the central region, by using shorter legs or larger voltage amplification.

Investigation as to whether the field dependence in μ is an emerging electrokinetic effect like that described by Bazant *et al.* [32,33] could be done by performing similar focusing experiments with increased field strength in the center (either by altering the nanofluidic device or using more powerful electronics), and extracting an estimate of μ_2 as we have done. If the emergence of μ_2 is induced by high ac fields, it is likely that the value of μ_2 will vary with the maximum field magnitude.

In the future, we intend to explore the degree of confinement dependence of μ_2 , up to measurements in free solution, to establish the slit-depth for several DNA contour lengths that optimizes the focusing effect. The frequency dependence of μ_2 requires further theoretical and experimental investigation. We would like to improve the resolution of our measurement by utilizing a stronger electric field to reduce the timescale of the experiments. This can be accomplished by reducing the length of the perpendicular legs connecting the central region to the reservoirs where the electrodes are inserted and by using higher voltage amplifiers. With moderate design improvements, we envision that the device could be used to selectively concentrate DNA within a narrow range of contour lengths in the central region, by utilizing the appropriate focusing frequency, for subsequent analysis either on or off chip.

VI. CONCLUSION

We have performed experiments demonstrating focusing and defocusing of λ DNA in nanoslits. Additionally, we extracted a first-order estimate of the nonlinear mobility term (μ_2) of the electrophoretic velocity (v) with the electric field strength (\vec{E}). Since we do not observe a focusing effect for a dipole rotation frequency of $>20 \text{ Hz}$, we infer that there is a μ_2 dependence on frequency that requires further investigation. We are fabricating new devices to measure μ_2 more accurately at various dipole rotation frequencies in the 1–100 Hz range. In the future, we intend to explore the confinement dependence of μ_2 for single DNA molecules within nanoslit devices and in free solution over a range of increased electric field magnitudes. We also intend to expand the size of the central region of our devices to facilitate single molecule study of focusing DNA.

ACKNOWLEDGMENTS

This work was performed in part at the Binghamton University Nanofabrication Facility and at the Cornell NanoScale Facility, a member of the National Nanotechnology Coordinated Infrastructure (NNCI), which is supported by the National Science Foundation (Grant No. NNCI-2025233). This research was supported by NSF Grant No. DMR-1351283.

All authors contributed equally to this work.

- [1] J.-L. Barrat and J.-F. Joanny, *Theory of Polyelectrolyte Solutions* (Wiley-Blackwell, Hoboken, 2007).
- [2] M. Muthukumar, 50th anniversary perspective: A perspective on polyelectrolyte solutions, *Macromolecules* **50**, 9528 (2017).
- [3] J. L. Viovy, Electrophoresis of DNA and other polyelectrolytes: Physical mechanisms, *Rev. Mod. Phys.* **72**, 813 (2000).
- [4] D. Stigter, Evaluation of the counterion condensation theory of polyelectrolytes, *Biophys. J.* **69**, 380 (1995).
- [5] D. A. Hoagland, E. Arvanitidou, and C. Welch, Capillary electrophoresis measurements of the free solution mobility for several model polyelectrolyte systems, *Macromolecules* **32**, 6180 (1999).
- [6] W. B. Russel, D. A. Saville, and W. R. Schowalter, *Colloidal Dispersions* (Cambridge University Press, Cambridge, 1989).
- [7] D. Andelman and W. C. Poon, *Soft Condensed Matter Physics in Molecular and Cell Biology* (Taylor & Francis, London, 2006).
- [8] G. S. Manning, Limiting laws and counterion condensation in polyelectrolyte solutions. 7. Electrophoretic mobility and conductance, *J. Chem. Phys.* **85**, 1506 (1981).
- [9] G. S. Manning, Limiting laws and counterion condensation in polyelectrolyte solutions: IV. The approach to the limit and the extraordinary stability of the charge fraction, *Biophys. Chem.* **7**, 95 (1977).
- [10] W. M. Gelbart, R. F. Bruinsma, P. A. Pincus, and V. A. Parsegian, DNA-inspired electrostatics, *Phys. Today* **53**, 38 (2000).
- [11] G. S. Manning and J. Ray, Counterion condensation revisited, *J. Biomol. Struct. Dyn.* **16**, 461 (1998).
- [12] W. Reisner, J. N. Pedersen, and R. H. Austin, DNA confinement in nanochannels: Physics and biological applications, *Rep. Prog. Phys.* **75**, (2012).
- [13] L. Dai, C. B. Renner, and P. S. Doyle, The polymer physics of single DNA confined in nanochannels, *Adv. Colloid Interface Sci.* **232**, 80 (2016).
- [14] K. D. Dorfman, DNA electrophoresis in microfabricated devices, *Rev. Mod. Phys.* **82**, 2903 (2010).
- [15] S. L. Levy and H. G. Craighead, DNA manipulation, sorting, and mapping in nanofluidic systems, *Chem. Soc. Rev.* **39**, 1133 (2010).
- [16] J. Tang, S. L. Levy, D. W. Trahan, J. J. Jones, H. G. Craighead, and P. S. Doyle, Revisiting the conformation and dynamics of DNA in slitlike confinement, *Macromolecules* **43**, 7368 (2010).
- [17] J. Tang, N. Du, and P. S. Doyle, Compression and self-entanglement of single DNA molecules under uniform electric field, *Proc. Natl. Acad. Sci. (USA)* **108**, 16153 (2011).
- [18] L. C. Campbell, M. J. Wilkinson, A. Manz, P. Camilleri, and C. J. Humphreys, Electrophoretic manipulation of single DNA molecules in nanofabricated capillaries, *Lab Chip* **4**, 225 (2004).
- [19] J. Pel, D. Broemeling, L. Mai, H. L. Poon, G. Tropini, R. L. Warren, R. A. Holt, and A. Marziali, Nonlinear electrophoretic response yields a unique parameter for separation of biomolecules, *Proc. Natl. Acad. Sci. (USA)* **106**, 14796 (2009).
- [20] A. Marziali, J. Pel, D. Bizzotto, and L. A. Whitehead, Novel electrophoresis mechanism based on synchronous alternating drag perturbation, *Electrophoresis* **26**, 82 (2005).
- [21] See Supplemental Material at <http://link.aps.org/supplemental/10.1103/PhysRevE.105.054503> for supplementary plots of $N + N$ versus time for μ_2 versus dipole frequency, and for the derivation of the drift velocity expression.
- [22] C. Sha, J. Hou, and H. Cui, A robust 2D Otsu's thresholding method in image segmentation, *J. Vis. Commun. Image Represent.* **41**, 339 (2016).
- [23] N. C. Stellwagen, C. Gelfi, and P. G. Righetti, The free solution mobility of DNA, *Biopolymers* **42**, 687 (1997).
- [24] J. D. Cross, E. A. Strychalski, and H. G. Craighead, Size-dependent DNA mobility in nanochannels, *J. Appl. Phys.* **102**, 024701 (2007).
- [25] G. B. Salieb-Beugelaar, J. Teapal, J. Van Nieuwkastele, D. Wijnperlé, J. O. Tegenfeldt, F. Lisdat, A. Van Den Berg, and J. C. T. Eijkel, Field-dependent DNA mobility in 20 nm high nanoslits, *Nano Lett.* **8**, 1785 (2008).
- [26] O. Castillo-Fernandez, G. B. Salieb-, J. W. van Nieuwkastele, J. G. Bomer, M. Arundell, J. Samitier, A. Van Den Berg, and J. C. T. Eijkel, Electrokinetic DNA transport in 20 nm-high nanoslits: Evidence for movement through a wall-adsorbed polymer nanogel, *Electrophoresis* **32**, 2402 (2011).
- [27] L. Wu and S. Levy, Fluctuations of DNA mobility in nanofluidic entropic traps, *Biomicrofluidics* **8**, 044103 (2014).
- [28] K. D. Dorfman and H. Brenner, Modeling DNA electrophoresis in microfluidic entropic trapping devices, *Biomed. Microdev.* **4**, 237 (2002).
- [29] A. C. Klepinger, M. K. Greenier, and S. L. Levy, Stretching DNA molecules in strongly confining nanofluidic slits, *Macromolecules* **48**, 9007 (2015).
- [30] G. W. Slater, C. Desruisseaux, S. J. Hubert, J. F. Mercier, J. Labrie, J. Boileau, F. Tessier, and M. P. Pépin, Theory of DNA electrophoresis: A look at some current challenges, *Electrophoresis* **21**, 3873 (2000).
- [31] D. W. Schaefer, J. F. Joanny, and P. Pincus, Semiflexible polymers in solution, *Macromolecules* **13**, 1280 (1980).
- [32] T. M. Squires and M. Z. Bazant, Induced-charge electro-osmosis, *J. Fluid Mech.* **509**, 217 (2004).
- [33] M. Z. Bazant, M. S. Kilic, B. D. Storey, and A. Ajdari, Towards an understanding of induced-charge electrokinetics at large applied voltages in concentrated solutions, *Adv. Colloid Interface Sci.* **152**, 48 (2009).